Expected wave loads along the flood protection system at Falsterbo Peninsula

Almström, Björn

2023

Document Version:
Publisher's PDF, also known as Version of record

LUNDS UNIVERSITET

LTH
LUNDS TEKNISKA HÖGSKOLA

Expected wave loads along the flood protection system at Falsterbo Peninsula

Internal scientific report
2023-12-01
Lunds Tekniska Högskola
Björn Almström

TABLE OF CONTENT

1 Introduction

This internal scientific report is a part of the Vinnova-project 'Nature-based protective dikes to flooding – planning, construction, and maintenance'. The overall goal with the project is to determine the wave resistance of the nature-enhanced revetment of the flood protection system planned at the Falsterbo peninsula.

The primary objective of this report is to assess the anticipated maximum wave loads impacting the planned Falsterbo flood protection system. Additionally, it outlines the methodology employed to estimate these wave loads, with an exclusion of the beach dune components within the protection system. The erosion resistance of beach dunes in the Falsterbo protection system is the central focus of the master thesis titled *'Storm Impact on Dunes in the Falsterbo Peninsula*' by Sukchaiwan (2023b).

In this study, we calculate wave loads on the dikes and seawalls by employing a nearshore wave model, which is supplemented with data from a regional wave model specific to the South Baltic Sea. The primary purpose of the nearshore model is to characterize the transformation of waves as they traverse from the open sea, crossing inundated areas, and reaching the flood protection structures.

The structure of this report entails an initial section describing the meteooceanographic conditions prevalent at the Falsterbo peninsula. Subsequently, we present the methodology, providing a comprehensive overview of the nearshore wave model and the input data utilized in this study. Finally, results are presented and analyzed while also limitations of this study are discussed.

1.1 Description of study site

The Falsterbo peninsula is situated in the southern Baltic Sea, an area characterized by prevailing short-period wind-generated waves primarily originating from the Arkona basin in the southwestern part of the Baltic Sea. Notably, this portion of the Baltic Sea is one of the shallowest regions, with an average depth of 23 meters and a maximum depth of 53 meters (Rosentau et al., 2017). High water events, in this area, are typically a consequence of seiching within the Baltic Sea. Seiches, or oscillations of water, manifest in the Baltic Sea due to storms pushing water toward the eastern or northern sections of the basin. When the wind subsides, this accumulated water is gradually released, giving rise to a seiche wave with a periodicity spanning 23 to 27 hours (Hanson & Larson, 2008). Consequently, it is noteworthy that high water events in the southern Baltic basin are not commonly associated with the immediate storm events but instead occur approximately 23 to 27 hours later.

Previous research has investigated the interplay between high water levels, wind patterns, and wave dynamics. In the study conducted by Hanson and Larson (2008), an extensive dataset covering the years 1982 to 2004 encompassing wind data from Falsterbo and water level measurements derived from Ystad and Simrishamn was analysed. This analysis incorporated wave hindcasting employing the simplified SMB formulation and various statistical methodologies. The findings of this study revealed that high water levels were associated to winds originating from the west-north-east sector. However, it was concluded that the strongest winds did not necessarily coincide with the high water levels.

For gale-force winds, characterized by speeds ranging from 14 to 24.4 meters per second, water levels exhibited fluctuations spanning from -1.10 meters to +0.8 meters. In cases of

storm winds, with velocities ranging from 24.5 to 32.6 meters per second, the water levels ranged between -0.4 meters and +0.4 meters. Additionally, Hanson and Larson (2008) demonstrated that when water levels reached +1.0 meter, the highest computed waves typically reached around 0.8 meters. This observation underscores the fact that high water levels and exceptionally large waves rarely coincide in this geographic region. Instead, the calculations suggest that the highest runup levels are predominantly the outcome of sizable waves coupled with relatively moderate water levels. Nonetheless, it remains imperative to account for wave dynamics during high water events, even if there is not a direct correlation between high water levels and substantial waves.

In an ocean-meteorological analysis of the Falsterbo peninsula conducted by Sweco (2018b), an investigation was carried out comparing the wind data series from Falsterbo to the water level records from the Skanörs hamn station. This analysis spanned the timeframe from 1992 to 2015. The findings indicated that northerly winds were the prevailing conditions during high water level events, and wind speeds of up to 15 meters per second were considered feasible. It's essential to note that this analysis encompassed a relatively brief period, which predominantly covered a period of relatively calm wind conditions. During this period, specific attention was given to wind speed and direction when water levels exceeded +1.0 meter (Figure 1). Among the observations, it was established that 35% of the recorded events featuring water levels surpassing +1.3 meters experienced wind speeds greater than 10 meters per second, while 6% of these events exhibited wind speeds exceeding 15 meters per second. This shows that moderate winds can appear during high-water events.

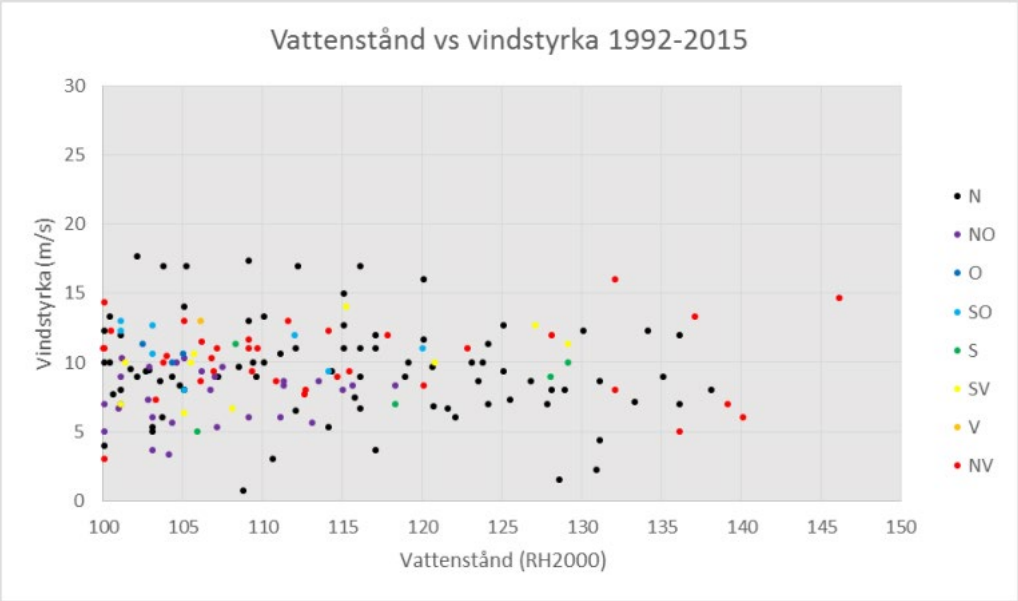

Figure 1. The scatter plot illustrates wind speeds associated with water levels exceeding +1.0 meter. Each data point is color-coded to represent the corresponding wind direction. This figure is sourced from Sweco (2018b).

Since the studies conducted by Hanson and Larson (2008) and Sweco (2018b), advancements have been made in the assessment of the long-term wave climate within the region. Particularly, this includes the development of a regional wave model specific to the southern Baltic Sea, as described in SGU (2021) and Adell et al. (2023). This regional wave model, validated through wave measurements conducted outside the Falsterbo peninsula, provides a comprehensive depiction of the wave climate spanning

from 1959 to 2021. The temporal resolution of this model was increased from 3 hours to 1 hour in Sukchaiwan (2023b) yielding better performance in describing waves heights during storm events.

Wave data was extracted from the regional wave model at three points north, south, and west of the Falsterbo Peninsula (Figure 2). At these points, maximum wave conditions for four different wind direction sectors and six wind speed intervals was collected and is presented **Table 1**. Largest waves are anticipated from the south where significant wave heights exceeding 4 m are simulated when southern or westerly winds are above 20 m/s.

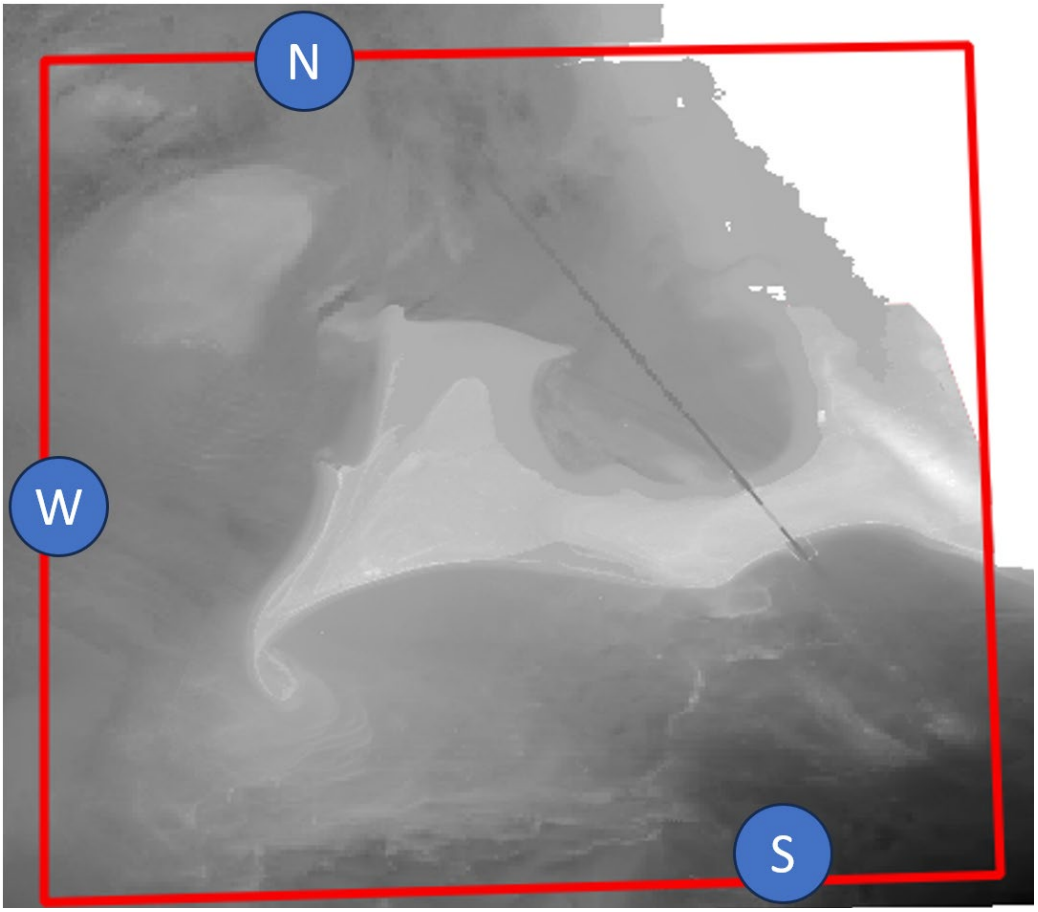

Figure 2. Bathymetry and topography in the study area. Darker colors represent greater depths, while brighter colors indicate higher elevations. The red frame outlines the nearshore model domain, and blue dots mark positions for wave data extraction from the regional model.

Table 1. *Wave conditions extracted from the regional model at the three boundaries (N,W,S) in the nearshore model*

Wind Direction	Boundary	Wind speed intervall																		
		0 - 5 m/s			5 - 10 m/s			10 - 15 m/s			15 - 20 m/s			20 - 25 m/s			> 25 m/s		
		H_s [m]	T_p [s]	Dir [°]	H_s [m]	T_p [s]	Dir [°]	H_s [m]	T_p [s]	Dir [°]	H_s [m]	T_p [s]	Dir [°]	H_s [m]	T_p [s]	Dir [°]	H_s [m]	T_p [s]	Dir [°]
N (315-45°)	N	0.66	6.1	215	0.93	8.1	215	1.59	4.8	265	1.55	4.6	265	-	-	-	-	-	-
	W	0.93	7.8	175	1.25	9.3	175	1.97	5.4	285	2.12	5.5	285	-	-	-	-	-	-
	S	2.25	7.6	125	1.91	8	125	2.22	8.8	115	2.09	6.1	265	-	-	-	-	-	-
E (45-135°)	N	0.71	7.5	205	1.06	8	215	1.23	7.8	215	-	-	-	-	-	-	-	-	-
	W	1.15	8.1	175	1.46	8	185	2.02	8.8	185	2.06	8.7	185	-	-	-	-	-	-
	S	1.88	7.9	125	2.66	7.2	125	3.54	8.7	125	3.8	8.5	125	-	-	-	-	-	-
S (135-225°)	N	0.82	6.5	215	1.34	6.6	215	1.88	7	225	2.24	6.8	225	-	-	-	-	-	-
	W	1.05	7.7	175	1.76	7.7	195	2.55	7.3	205	3.13	7.4	205	2.99	7.2	205	-	-	-
	S	1.9	7.5	125	2.42	7.9	125	3.5	8	135	3.69	8	185	4.12	7.3	185	-	-	-
W (225-315°)	N	0.81	6.4	215	1.5	6.2	225	1.92	7.1	225	2.34	6.6	235	2.4	7.2	225	-	-	-
	W	1.14	6.8	195	1.81	6.7	205	2.47	6.8	205	3.01	7.3	205	3.32	7.7	215	-	-	-
	S	1.69	7.8	125	2.24	7.5	185	3.09	8	185	3.78	8.1	185	4.43	7.7	185	-	-	-

Waves extracted from the regional wave model are compared with observed still water levels at SMHI:s station Klagshamn (Figure 3). The largest waves are seen at the south boundary, with significant wave heights up to 4 m, while the smallest waves are found at the north boundary, where significant wave heights reach up to 2.5 m. Large waves coincide with still water levels up to +1.0 m. However, when the still water levels exceed +1.0 m there is a sharp decline in wave heights (Figure 3). For the North boundary the significant wave heights barely exceeds 1.0 m for such still water levels, whereas at the south boundary, waves reach nearly a height of 2 m, and at the west boundary waves reaches heights up to 1.5 m. These findings confirm the results from Hanson and Larson (2008), emphasizing that extreme still water levels and extreme waves do not coincide. Nonetheless, it is noteworthy that the regional wave model and the study of Hanson and Larson (2008) shows that notable wave heights are present during extreme still water levels.

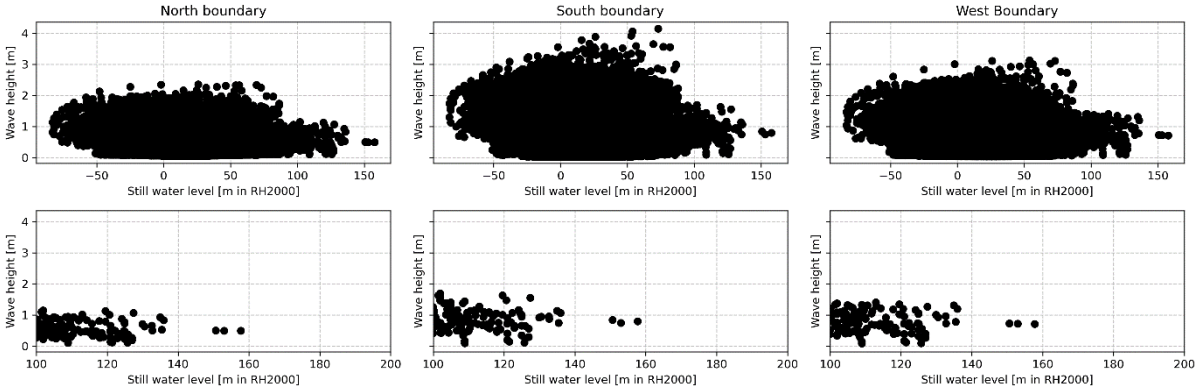

Figure 3. Waves extracted at the boundaries (North, South, and West) versus observed water level at SMHI:s station Klagshamn. The lower subplots show waves for still water levels exceeding +1.0 m.

An extraordinary occurrence where waves correlated with a storm surge occurred during the 'Backafloden' storm in 1872. This severe storm wrought extensive destruction along the southwestern Baltic Sea coast, affecting Denmark, Germany, and Sweden. The uniqueness of this event was attributed to an unusual interplay of pressure systems, as described by Feuchter et al. (2013). In the days leading up to the storm, westerly winds

pushed water into the Baltic Sea. A high-pressure system was established over Scandinavia while a low-pressure system moved in over central Europe. This generated north-easterly to easterly winds reaching hurricane strength. The winds pushed water to the southwestern basin of the Baltic Sea and extreme waves were generated by strong wind. Resulting in the extreme water levels coinciding with the extreme waves for the 1872-storm.

Unfortunately, at the time of the storm, there were no stations recording the water levels along the Swedish south coast. The still water level along the Swedish coast during the storm is therefore unknown. However, Germany and Denmark did have stations measuring the still water levels at the time of the storm. In Travemünde, Germany, the still water level was observed to +3.4 m above mean sea level, while in Köge, Denmark, the sea level reached +2.8 m above mean sea level. Considering the wind direction and the geographical shape of the southern Baltic Sea basin, it is presumed that the still water level along the Swedish coast during the storm would have been lower.

In an attempt to estimate the storm surge level at the Falsterbo peninsula during the 1872-storm, Fredriksson, Tajvidi, et al. (2016) reconstructed the water level by going through historical records and surveying the waterline of the memory stone for the 1872-storm. They estimated the still water level to be +2.4 m above mean sea level, corresponding to +2.6 m in the Swedish national height system (RH2000). This estimation was based on measurements of a memorial stone over the 1872-storm located in the Falsterbo peninsula and on previous studies of the water level during the storm.

Waves during the 1872-storm were simulated in a study conducted by Sukchaiwan (2023a) using the regional wave model from Adell et al. (2023) and winds reconstructed by Rosenhagen and Bork (2009). From the model of Sukchaiwan (2023a) waves were extracted at the North, South, and West boundary (Figure 2) and the maximum wave condition are presented in Table 2:

Table 2. Simulated Maximum waves under 1872-storm (Sukchaiwan, 2023a) at the boundaries North, South, and West (Figure 2).

Boundary	**Depth** [*m*]	**Hs** [*m*]	**Tp** [*s*]	**Dir** [*deg. N*]
North	8.3	2.69	6.0	26
South	17.6	4.89	10.7	111
West	9.9	3.07	6.2	14

The 1872 storm represented a highly unusual event within the Baltic Basin, primarily due to the unprecedented water levels it generated. Equally unique was the synchronization of extreme waves with these exceptional water levels. This storm serves as a potent reminder that scenarios beyond the scope of our brief observational records can occur. Relying on observed events alone might inadvertently exclude scenarios that could happen, even if they have not been witnessed.

Therefore, when developing a methodology for estimating wave loads on the flood protection system at the Falsterbo peninsula, it is imperative not to solely depend on methods simulating statistically probable events. A comprehensive approach should encompass the potential for rare and extreme scenarios, as demonstrated by the historical 1872 storm, to ensure the robustness and resilience of the flood protection system.

2 Methodology

Previous studies of wave conditions along the Falsterbo peninsula have mainly focused on the correlation, or the lack thereof, between high water levels and large waves. Nevertheless, it's essential not to misinterpret this absence of correlation as an indication that waves are entirely absent during high-water events. For example, Sweco (2018b) stated that winds of 15 m/s are plausible during a high-water event, which would generate local waves. Moreover, as indicated in **Table 1**, waves are present even under calm wind conditions. Therefore, waves could theoretically coincide with high-water level event. Additionally, given the limited historical records of winds and water levels along the south of coast of Sweden, it is probable that combinations of wind watter levels have occurred but without being observed. Consequently, this study aims to investigate wave loads along the flood protection system for high-water events under various wind conditions.

The overarching methodology for this study involves employing a nearshore model of the Falsterbo peninsula, which encompasses dry land expected to be flooded, to simulate the incipient waves on the flood protection structure across multiple scenarios. These scenarios combine offshore wave input data extracted from the regional model with varying wind directions and wind speed. The outcome of these simulation will yield a database comprising anticipated wave condintions at specified output points along the dikes and seawalls.

2.1 Nearshore wave model

The nearshore waves were simulated using the open-source software SWAN (Booij et al., 1999), version 41.45. SWAN is a state-of-the-art wave model widely employed globally in both research and practical applications. The model is a third-generation spectral wave model capable of resolving:

- wave propagation and generation for deep and shallow water in time and space due to shoaling,
- refraction,
- wave interaction with currents and bottom, and
- frequency shifting due to currents and non-stationary depths.

In the model, waves are generated by transferring energy from the wind to the waves. The dissipation of wave energy in the model is attributed to white-capping, bottom friction, and depth-induced breaking. Additionally, the model has the capability to include dissipation effects from aquatic vegetation and, to some extent, resolve diffraction processes.

Computations in SWAN can be conducted on either a regular, curvilinear, or a triangular mesh. For this study, a triangular mesh was selected to achieve finer resolution in shallow areas, allowing for the accurate representation of wave propagation processes. The mesh for the nearshore model was generated using open-source scripts from OceanMesh 2D (Roberts et al., 2019). The mesh resolution ranged up to 250 m in offshore areas, up to 100 m in areas with an elevation between -2 m and +1 m, and up to 50 m in areas with an elevation exceeding +1 m

The nearshore model was run with 36 directional bins and 38 frequency bins, equally spaced within the range of 0.05-1 Hz. The model employed default parameters with the additional activation of depth induced wave breaking in shallow water using the BKD-

scheme, which allows the breaker index to be scaled based on bottom slope and the dimensionless depth. Furthermore, bottom friction was included in the model as a JONSWAP with a constant bottom friction coefficient of 0.038 m^2/s^3, typical of sandy bottoms. Additionally, the model accounted for the triad wave-wave interaction and an approximation for accounting for diffraction processes. Wave dissipation from vegetation was not considered in the current model due to absence of vegetation data.

2.1.1 Input data

The SWAN model requires information concerning bathymetry, boundary conditions (e.g. incoming waves at offshore boundaries), and wind forcing. Details regarding the input data utilized in this study are provided in Section 2.1.1 ‘Input data’.

Depth and elevation within the model were compiled using three different data sources. The most recent LiDAR-survey conducted by Lantmäteriet (eng. The Land Survey) in 2018, with a resolution 1x1 m, was combined with SGU’s (eng. the Swedish Geological Survey) multibeam scanning, with a resolution of 2x2 m, for nearshore bathymetry within the depth range of 0-6 m, and the European Marine Observations and Data Network (EMODnet) bathymetry portal, with a resolution of 115x115 m, for depths exceeding 6 m. The combined data was then interpolated to create a digital elevation model (DEM) with a 2x2 m resolution. The SWAN-model extract depth data from this DEM at the computational nodes within the mesh, resulting in varying depth resolutions throughout the model domain.

Boundary conditions encompass both offshore boundaries, where waves enter the nearshore model, and shoreline boundaries where all wave energy is dissipated. The wave input specification at these boundaries is detailed in **Table 1** for the various wind condition scenarios. The shoreline boundaries are delineating areas not of interest to the study, i.e., north and south of the Falsterbo peninsula. The shoreline boundary is determined based on the actual shoreline, with the exception of the Falsterbo peninsula where the shoreline is defined as the position of the flood protection system. Information regarding the location the flood protection system sourced from Sweco (2023).

Figure 4. Type of structure for the flood protection system: dike (green line), seawall (black line), and yet not decided (green/black line).

2.1.2 Output data

Significant wave heights, period, and direction are extracted from the nearshore wave model at intervals of 100 m along the dike and at a distance of 25 m from the dike. The distance from the dike is done to avoid boundary effects in the nearshore wave model. Furthermore, the flood protection was subdivided into segments according to their geographical location, facilitating the aggregation of simulation results to the various segments of the flood protection site (Figure 5).

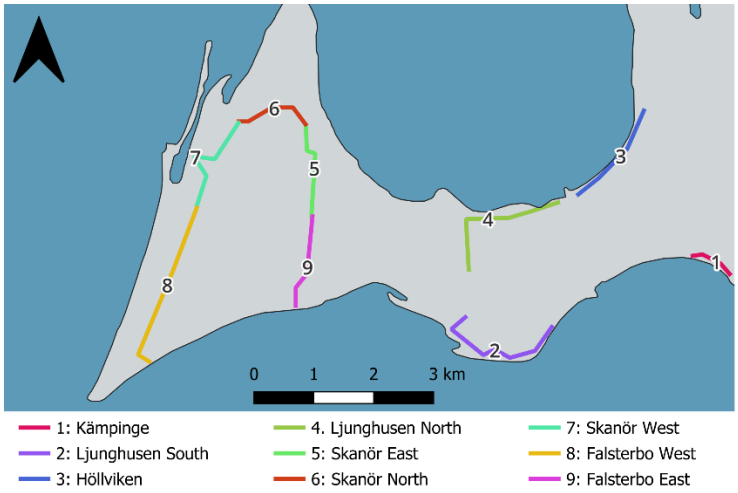

Figure 5. Segment division of the flood protection system and names that is referred to hereafter.

2.2 Scenarios

Multiple scenarios were simulated using the nearshore wave model to generate wave data for various wind conditions and extreme water levels. In total, 42 scenarios were simulated, encompassing 21 different wind scenarios for two different still water levels:

- A still water level with a 100-year return period, denoted as HW100. In Fredriksson, Tajvidi, et al. (2016), the HW100 was estimated to be +1.81 m (in RH2000) based on an extreme value analysis (GEV) of a water level series that combined the Klagshamn, Ystad and Falsterbo time series.
- The estimated still water level during the 1872-storm, referred to as 1872-storm, which was +2.6 m (RH2000) as taken from Fredriksson, Tajvidi, et al. (2016).

These still water levels refer to present day climate. However, the flood protection system at Falsterbo has a life expectancy until the year 2065. Consequently, the expected sea level until the year 2065 must be included in the scenarios. Until the year 2065 the sea level is expected to rise with 0.5 m. Hence, the still water level of HW100 and 1872-storm were adjusted upwards by 0.5 m to account for the projected the sea level rise. This results in the still water level for HW100 and the 1872-storm being +2.31 m (RH200) and +3.10 m (RH2000), respectively.

For each water level, wind blowing from four different sectors (as outlined in Table 3) - North, East, South, and West - was simulated. Wind speeds of 5, 10, 15, 20, and 25 m/s were included for each wind direction sector. Additionally, the highest offshore wave conditions from the regional wave model were incorporated for each wind combination (see **Table 1**).

Table 3. Scenarios simulated with the nearshore wave model.

Still water level, year 2065	**Wind direction**	**Wind speed** [*m/s*]				
HW100 (+2.31 m in RH2000)	North (0°)	5	10	15	20	25
	East (90°)	5	10	15	20	25
	South (180°)	5	10	15	20	25
	West (270°)	5	10	15	20	25
1872-storm (+3.10 m in RH2000)	North (0°)	5	10	15	20	25
	East (90°)	5	10	15	20	25
	South (180°)	5	10	15	20	25
	West (270°)	5	10	15	20	25

3 Results

Results from the nearshore model have been aggregated according to segments of the flood protection system (Figure 5). In Appendix 1, the maximum wave load at each segment is tabulated for all the simulated scenarios. The simulations indicate that waves are consistently present at the flood protection system in every scenario, and the wave height increases with wind speed and still water level (Figure 6).

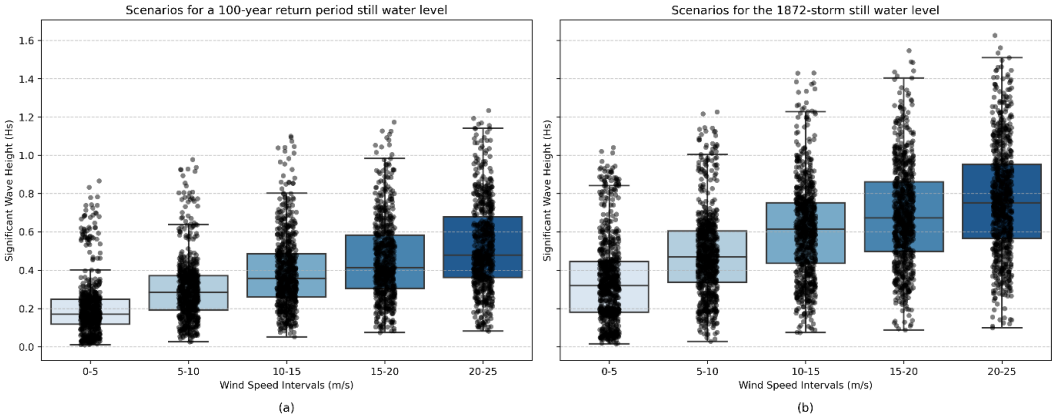

Figure 6. Box plots illustrating wave characteristics at the flood protection site within different wind speed intervals. Each box plot displays the median wave height (second quantile), along with the 25th and 75th percentiles, while individual data points (dots) represent observed wave heights. (a) Simulations with a still water level corresponding to a 100-year return period, factoring in climate change projections for the year 2065. (b) Results based on a still water level corresponding to the 1872-storm, considering climate change projections for the year 2065

Furthermore, the water depth (or ground elevation) seaward of the flood protection system is also a factor that influence wave height (Figure 7). Deeper water (or lower elevation) seaward of the dike allows larger waves to impact on the flood protection system.

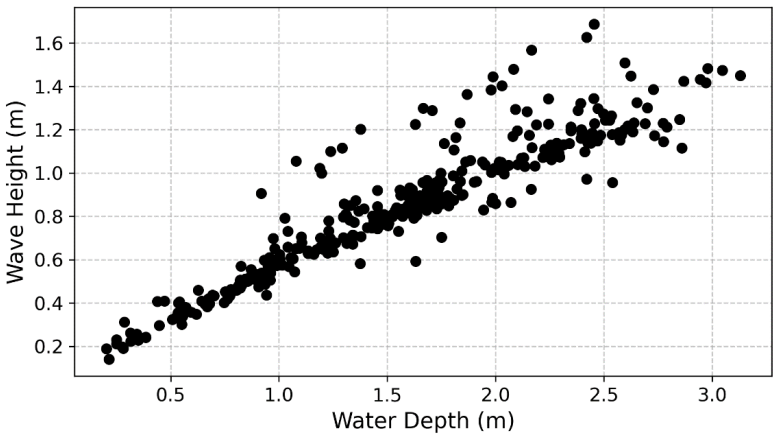

Figure 7. Simulated maximum wave height along the flood protection system as function of the water depth considering all scenarios.

3.1 Maximum expected wave heights

In Figure 8 and Figure 9, the maximum significant wave height are displayed for every 100 m along the flood protection system. In the HW100 scenarios (Figure 8), the anticipated waves heights are lower than in the 1872-storm scenarios (Figure 9). The largest maximum wave heights for HW100 (Figure 8) are observed along Höllviken, eastern section of Ljunghusen North, and Kämpinge. Along these segments, waves can reach heights up to 1.3 m at the toe of the flood protection system. Wave heights measure 0.2 m or larger at almost all locations along the flood protection system, except for a few points where the water depth of the dike is very small due to the topography in relation to the still water level.

For the 1872-storm scenarios, the waves in front of the flood protection system are notably larger. The segments of Kämpinge, Höllviken, parts of Ljunghusen North and South receives the largest waves in this scenario as well. However, in these scenarios, Skanör West and Falsterbo West, also have large waves seaward of the flood protection system. The latter ones can however be a result of the model not fully describing the topographic of the beach dunes in front of these areas.

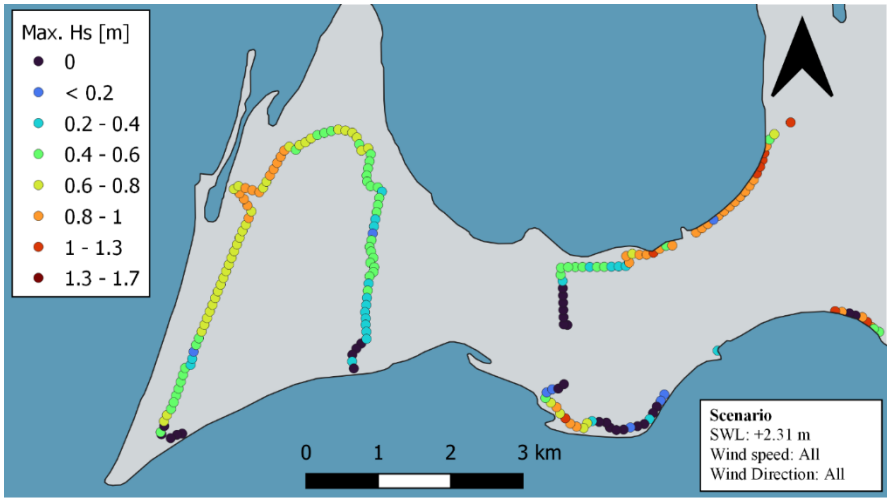

Figure 8. Maximum significant wave heights for scenarios with a still water level corresponding to the 100-year flood in the year 2065.

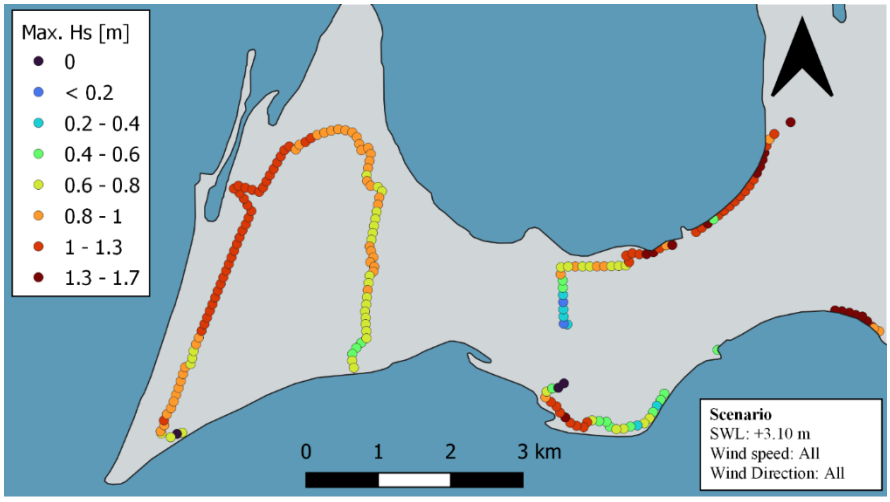

Figure 9. Maximum significant wave heights for scenarios with a still water level corresponding to the 1872-storm adjusted with expected sea level rise until the year 2065.

3.2 Maximum expected wave heights during wind less than 15 m/s

In the environmental application for the flood protection system Sweco (2018b) indicated that while storm winds are unlikely to coincide with a storm surge, it is plausible that winds of up to 15 m/s may occur simultaneously with a storm surge. Consequently, the analysis of the flood protection system's resistance in the environmental application primarily focused on this particular scenario. It is therefore of show the results from the nearshore model for this scenario (Figure 10 and Figure 11).

In comparison to the results obtained for all wind speeds, the higher wave heights are reduced in a scenario with maximum wind speed of 15 m/s. However, for output points with lower wave heights there is less, or none, reduction. This because of shallow water depths at these locations limits the wave heights in all scenarios.

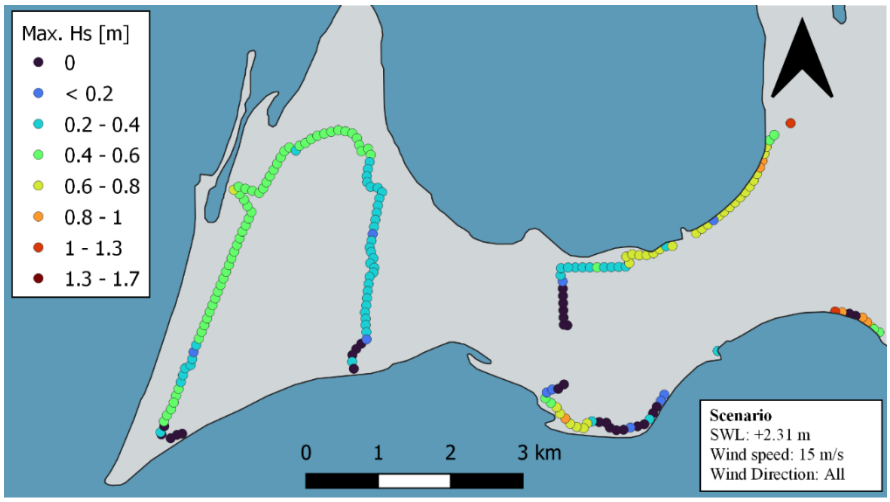

Figure 10. Maximum significant wave heights along the flood protection system for a still water level corresponding to HW100 (+2.31 m in RH2000) and wind speeds up to 15 m/s.

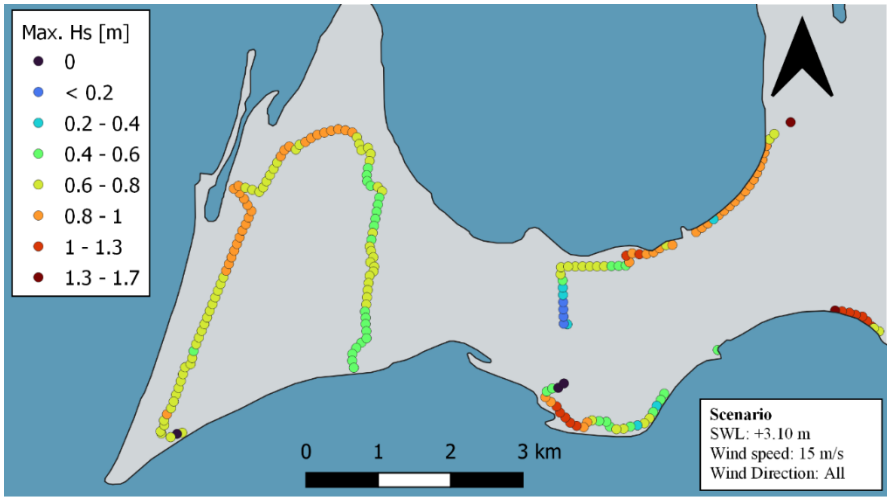

Figure 11. Maximum significant wave heights along the flood protection system for a still water level corresponding to the 1872-storm (+3.10 m in RH2000) and wind speeds up to 15 m/s.

3.3 Wave run-up and overtopping

The maximum elevation that waves reach will be higher than wave amplitude due to waves will run up on the dike slope. This is called wave run-up. If the wave run-up is higher than the crest of the dike, the wave will pass over the dike. Wave run-up and overtopping can be estimated using empirical formulations in the EurOtop (2018). EurOtop is considered as an industry standard within Europe for designing coastal defences in terms of wave run-up and overtopping.

Wave run-up in EurOtop (2018) is defined as the height only exceeded by 2% of the waves. For grass covered dike slopes gentler than 1:2, the mean value for the wave run-up is calculated using:

$$\frac{R_{u2\%}}{H_{m0}} = 1.65\gamma_b\gamma_f\gamma_\beta\varepsilon_{m-1,0} \quad (1)$$

With a maximum of:

$$\frac{R_{u2\%}}{H_{m0}} = 1.0\gamma_f\gamma_\beta\left(4 - \frac{1.5}{\sqrt{\gamma_b - \varepsilon_{m-1,0}}}\right) \quad (2)$$

Where $R_{u2\%}$ is the wave runup height above still water level, H_{m0} is the spectral significant wave height at the toe of the structure, γ_b is the influence factor for a berm (no berm, $\gamma_b = 1$), γ_f is the influence factor for roughness on the slope (grass on slope, $\gamma_f = 1$), γ_β is the influence factor for oblique waves (for conservative assessment assumed to be 1), and $\varepsilon_{m-1,0}$ is the surf similarity given by:

$$\varepsilon_{m-1,0} = \frac{\tan\alpha}{\sqrt{H_{m0}/L_{m-1,0}}} \quad (3)$$

Where $tan(\alpha)$ is the slope and $L_{m-1,0}$ is the deep-water wavelength based on the spectral period.

The overtopping discharge in EurOtop (2018) are given by the mean value approach:

$$\frac{q}{\sqrt{gH_{m0}^3}} = \frac{0.023}{\sqrt{\tan\alpha}}\gamma_b\varepsilon_{m-1,0}e^{\left(-\left(2.7\frac{R_C}{\varepsilon_{m-1,0}\cdot H_{m0}\cdot\gamma_b\cdot\gamma_f\cdot\gamma_\beta\cdot\gamma_v}\right)^{1.3}\right)} \quad (4)$$

With a maximum of:

$$\frac{q}{\sqrt{gH_{m0}^3}} = 0.09\cdot e^{\left(-\left(1.5\frac{R_C}{H_{m0}\cdot\gamma_b\cdot\gamma_f\cdot\gamma_\beta\cdot\gamma^*}\right)^{1.3}\right)} \quad (5)$$

Where q is the mean discharge per meter, g is the acceleration due the gravity, R_c is the crest freebord, γ_v is the influence factor for a wall in the end of a slope (γ_v=1 if no wall), and γ^* is the combined influence factor (γ^*=1 for standard dike design)

Tolerable mean overtopping on a grassed covered slope is indicated by EurOtop (2018), see Table 4.

Table 4. Tolerable mean discharge of various types grass covered slopes (EurOtop, 2018)

Type	**Mean overtopping discharge** [l/s/m]
Grass covered crest and landward slope, maintained and closed grass cover (H_{m0} = 1-3 m)	5
Grass covered crest and landward slope; not maintained grass cover, open spots, moss, bare patches (H_{m0} = 0.5 – 3 m)	0.1
Grass covered crest and landward slope (H_{m0} < 1 m)	5-10
Grass covered crest and landward slope (Hm0 < 0.3 m)	No limit

A majority of the output points along the flood protection system have a runup level exceeding the crest height of the flood protection system (Figure 12). The runup levels have been calculated assuming a grass covered dike with slope of 1:3 and is therefore only valid for those locations where a dike is planned to be a part of the flood protection system.

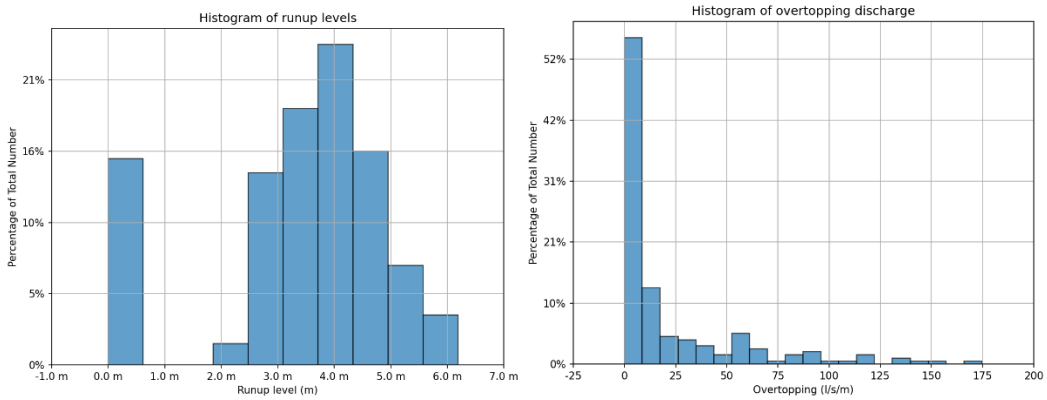

Figure 12. Histogram of runup levels (left), and mean discharge from overtopping (right)

In Figure 13 the calculated runup levels along the flood protection system is shown and in Figure 14 the mean discharge due to overtopping is shown. The color gradation in Figure

14 is based on the tolerable discharge for a grass dike in Table 4. Possibility of breach is high for discharges above 0.1 l/s/m depending on the resistance of the vegetation cover and all grass covered dike are likely to breach for discharge over 10 l/s/m.

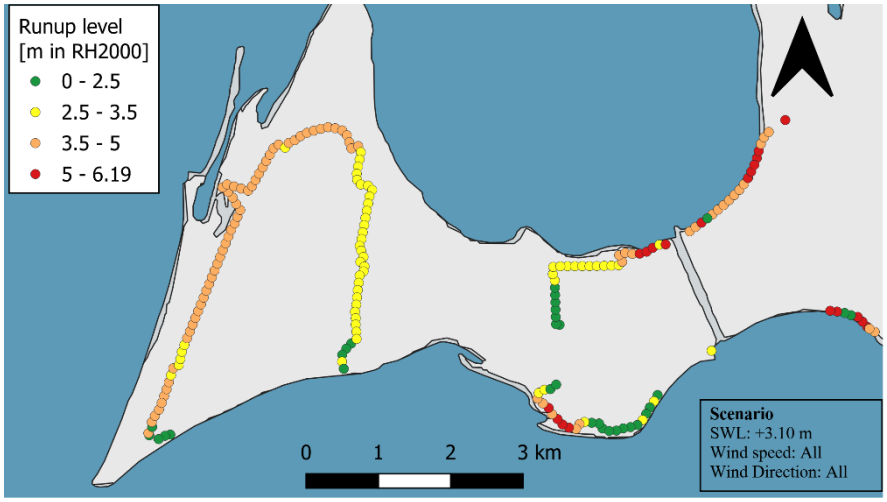

Figure 13. Runup levels (in RH2000) assuming a grass covered dike slope of 1:3 along the flood protection system

Figure 14. Mean discharge from overtopping assuming a grass covered dike slope of 1:3 along the flood protection system

3.4 Wave load

Wave load on the dike have been assessed using the maximum impact pressure from a plunging breaker. A plunging breaker represents the worst-type of the breaking waves on the outer slope in terms of breaching. The wave energy asserted onto the slope from a plunging breaker is dissipated over a short distance and within short time, resulting in a relatively small surface area exposed for a very short period of time to a high impact pressure (Stanczak, 2008). The wave load from breaking waves do not act continuously, but intermittently in time intervals of at least on wave period. Often longer time intervals than one wave period is expected due to the predominant impact on the water layer due to the wave up and down rush processes of the proceeding wave. Additionally, entrained

air results in large variations of the wave breaking process. Parameters describing this process must therefore be described stochastically.

The maximal impact pressure represents a stochastic variable and is therefore defined in this study as the pressure not is not exceeded by 99.9% of the waves, noted by $p_{max,\ 99.9\%}$. In practice, $p_{max,\ 99.9\%}$ is considered as the highest maximum pressure (Stanczak, 2008).

In accordance with Stanczak (2008) the maximal impact pressure was calculated using the approach by Zhong (1985):

$$p_{max,99.9} = \kappa_{99.9}\rho_w g H \tan\alpha \qquad (1)$$

With ρ_w is the density of water, g acceleration due to gravity, H is the wave height, tan α is the slope of dike, $\kappa_{99.9}$ is an empirical coefficient that depends on the deep water wave steepness

$$\kappa_{50} = -289\frac{H}{gT_p^2} + 11.2 \qquad (2.1)$$

$$\kappa_{99.9} = -289\frac{H}{gT_p^2} + 11.2 \qquad (2.2)$$

The maximum impact pressure ranged from 8.7 to 108.1 kPa with most dike locations within the maximal impact pressure of 30 to 60 kPa (Figure 12).

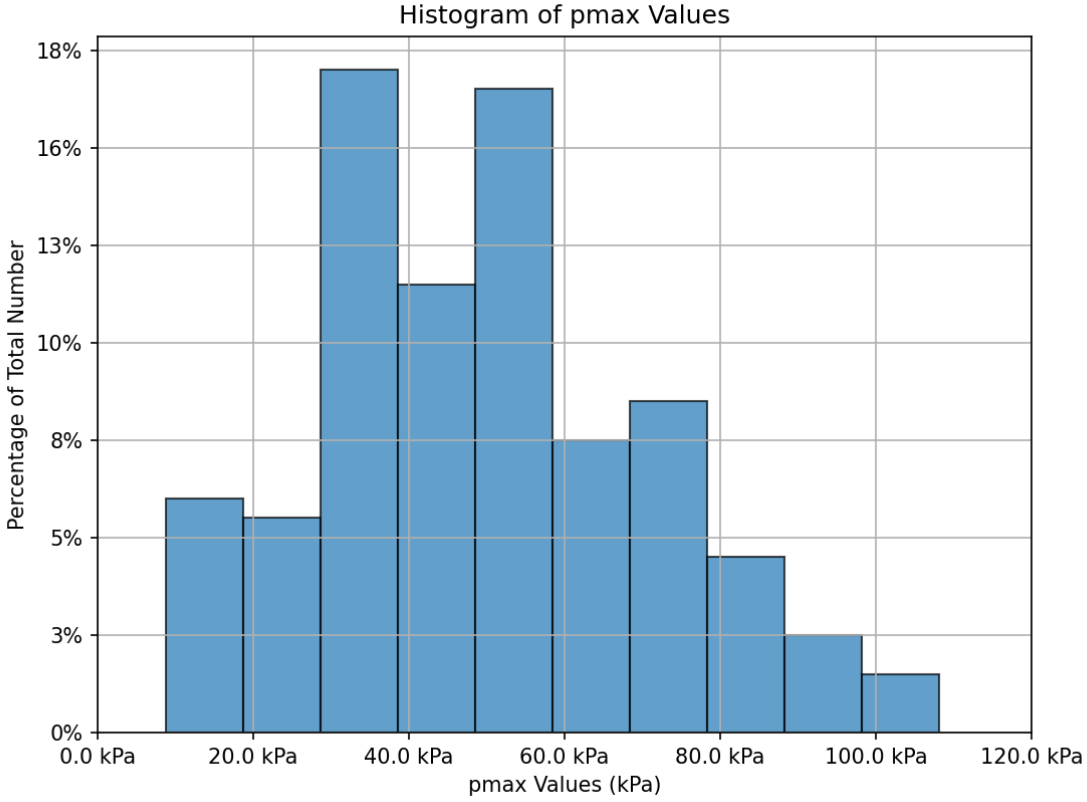

Figure 15. Histogram of the calculated maximum wave impact pressure along the flood protection system.

4 Discussion and conclusion

The nature-based revetment installed on the dike segments of the flood protection system at the Falsterbo Peninsula must be able to withstand the anticipated wave loads exerted upon it. Failure to do so could lead to wave-induced damage, potentially resulting in breaches of the dikes with possible catastrophic consequences.

The design of the dike segments has not taken into account any specific event, and the technical description of the environmental permit application does not include calculations for the erosion resistance of the nature-based revetment (Sweco, 2018a). Hence, it is essential to assess the erosion resistance of the nature-based revetment. To accomplish this, it is imperative to have knowledge about the expected wave loads acting upon the dike segments. The wave loads are strongly influenced by the water depth at the toe of the dike, as demonstrated in this study (see Figure 7). Therefore, the choice of still water level in the scenarios will greatly influence the final outcome from the simulations.

In the environmental permit application (Sweco, 2018c) two types of scenarios for the still water level are mentioned: one still water level corresponding to a 100-year return period, factoring in the sea level rise projected until the year 2065, and the other with a still water level corresponding to the conditions during the 1872-storm, also accounting for the expected sea level rise until 2065. In this study, the still water levels for these two scenarios are +1.81 m and +2.60 m in RH2000, respectively. These levels are derived from an extreme value analysis of water level at the Falsterbo Peninsula and historical assessment of the still water level during the 1872-storm (Fredriksson, Tajvidi, et al., 2016).

In this part of the Baltic Sea basin, extreme water levels do not typically coincide with extreme waves; however, they do coincide with waves (Hanson & Larson, 2008). This was further validated by extracting wave data from the regional wave model and aligning it with the water levels records from SMHI:s station Klagshamn (Figure 3). Simulations indicate that waves with a significant wave height up to 2 m have occurred for still water levels exceeding +1.0 m. Moreover, for still water levels surpassing +1.5 m, waves heights up to 1 m can be observed. Nevertheless, the very most extreme water levels are align with extreme water levels. An example of such event is the 1872-storm. Sukchaiwan (2023a) conducted simulations to assess wave conditions during the 1872-storm using a reconstructed wind field. The study showed that the storm generated significant wave heights up to 4.9 m south of the Falsterbo Peninsula.

As these offshore waves propagate towards the flood protection system they will transform as they interact with the bottom. To account for this transformation, a nearshore wave model covering the Falsterbo Peninsula was developed using the numerical wave model SWAN. The wave condition along the protection system were simulated using two scenarios for the still water level in combination with wind speeds of 5, 10, 15, 20, 25 m/s from the north, west, south, and east directions. In this approach, the maximum waves from the regional wave model for each wind scenario were extracted at the boundaries of the nearshore model. This approach does not provide a likelihood of a specific wave load, but it does offer a valuable insight into the types of wave loads that can be expected under various wind conditions.

The results show that in both water level scenarios, the flood protection system is exposed to waves, even in scenarios with wind speeds of as low as 5 m/s. On average, significant wave heights in front of the flood protection system are approximately 0.5 m, but can reach up to 1.3 m for a still water of +2.31 m (HW100). In the 1872-storm scenarios, the average significant wave height is approximately 0.8 m with a maximum value of 1.7 m.

The results from the simulations cannot be validated due to the absence of available wave measurements at Falsterbo peninsula during extreme water levels. Instead, the results can be compared with another study that investigated runup levels at six different locations along the flood protection system for a still water level of +2.86 m (in RH2000) and onshore wind of 25 m/s using the numerical model SWASH (Fredriksson, Hanson, & Larson, 2016). The simulated wave heights at these six different locations are compared in Table 4 between the two studies. Despite the slight variations in the scenarios used in the two studies, the magnitude of the wave height is comparable. This suggest that the results of the present study fall within expected range.

Table 5. Comparing simulated significant wave heights from SWASH Fredriksson, Hanson and Larson (2016) were SWASH was used and from this study using SWAN. Overview map of the transect location is excerpted from Fredriksson, Hanson and Larson (2016).

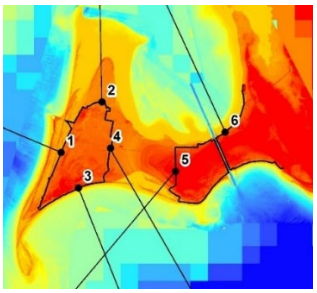

Transect	SWASH	SWAN
1	0.97 m	1.02-1.05
2	1.21 m	0.95-0.99
3	1.38 m	-
4	1.04 m	0.76-0.81
5	-	-
6	0.79 m	1.1-1.4 m

For the upcoming field experiments assessing the erosion resistance of the nature-enhanced revetment, it is recommended to focus primarily on the wave conditions associated with the HW100-scenarios, as the still water level in the 1872-storm scenario exceeds the crest level of flood protection system. Additionally, parts of the flood protection system will consist of seawalls. Therefore, the field experiments should specifically target wave loads at the segments where a dike is intended to be constructed (Figure 4). The maximum wave height along these segments, where a dike is planned, corresponds to a wave with the following characteristics: significant wave height = 1.2 m, peak wave period = 5.0 s, and wave direction =343°

4.1 Uncertainties/Limitations and Future work

There are several known uncertainties and limitations associated with the chosen methodology for this study that should be taken into consideration when interpreting the results:

1. **Lack of probability estimations of the scenarios**: The scenarios used in this study are not linked to specific probabilities of occurrence, making it challenging to relate wave heights to a specific return period. This limitation arises from the limited time series available for ocean-meteorological conditions at Falsterbo, which restricts the types of extreme events that have been recorded. Statistical analysis of longer time series would likely yield scenarios where high-water levels, strong winds, and high waves are not combined. However, historical storm descriptions indicate that events involving the simultaneous occurrence of high-water levels, large waves, and strong winds have occurred. It is, therefore, valuable to include such events in an analysis of wave loads on the flood protection system, even if they have not happened in the recorded data.

Overcoming this limitation would require significantly longer time series encompassing multiple high-water level events.

2. **Lack of Validation Data**: The accuracy of the simulated wave heights is unknown due to the absence of validation data. Validating the model would require wave measurements during events where parts of Falsterbo is flooded, which have not occurred during the course of this project. However, it is worth noting that the regional wave model used in this study has been validated against wave measurements outside the southern part of the Falsterbo peninsula (Adell et al., 2023). Additionally, the SWAN model has been validated in numerous scientific studies worldwide.
3. **Wave Dissipation Due to Vegetation**: The present model does not account for wave dissipation caused by vegetation. As a result, it may overestimate wave heights in areas with a long and shallow foreshore between the flood protection system and the shoreline. This limitation is expected to be more pronounced in areas where the foreshore is densely vegetated with forests or bushes. Future work on the nearshore wave model should focus on incorporating wave dissipation due to vegetation.
4. **Resolution of Mesh**: The model's mesh resolution may be insufficient in areas with rapid changes in topography, such as dune areas. This can lead to the exclusion of dune and other topographic features that could significantly reduce wave heights. The segments Falsterbo West and Skanör West may be particularly affected by this lack of resolution, potentially resulting in overestimated wave heights. However, the morphologic evolution of the dunes up to the year 2065 is highly uncertain, and it is unclear which of the simulated scenarios the present-day dunes would be able to withstand. The absence of a finer mesh in relevant areas is due to a limitation with the mesh generator used in this study. Future improvements to the nearshore model should prioritize creating a finer mesh in such areas.

These limitations should be taken into account when interpreting the findings of this study and may serve as areas for further research and model refinement in future investigations.

References

Adell, A., Almström, B., Kroon, A., Larson, M., Uvo, C. B., & Hallin, C. (2023). Spatial and temporal wave climate variability along the south coast of Sweden during 1959–2021. *Regional Studies in Marine Science*, *63*, 103011. https://doi.org/https://doi.org/10.1016/j.rsma.2023.103011

Booij, N., Ris, R. C., & Holthuijsen, L. H. (1999). A third-generation wave model for coastal regions: 1. Model description and validation. *Journal of Geophysical Research: Oceans*, *104*(C4), 7649-7666. https://doi.org/https://doi.org/10.1029/98JC02622

EurOtop. (2018). *Manual on wave overtopping of sea defences and related structures. An overtopping manual largely based on European research, but for worldwide application* (J. W. Van der Meer, N. W. H. Allsop, T. Bruce, J. De Rouck, A. Kortenhaus, T. Pullen, H. Schüttrumpf, P. Troch, & B. Zanuttigh, Eds. Second Edition ed.). www.overtopping-manual.com

Feuchter, D., Jörg, C. S., Rosenhagen, G., Auchmann, R., Martius, O., & Brönnimann, S. (2013). The 1872 Baltic Sea storm surge.

Fredriksson, C., Hanson, H., & Larson, M. (2016). *PM Dimensionering av krönhöjd för översvämningsskydd Falsterbohalvön*.

Fredriksson, C., Tajvidi, N., Hanson, H., & Larson, M. (2016). Statistical analysis of extreme sea water levels at the Falsterbo peninsula, South Sweden. *VATTEN – Journal of Water Management and Research*, *72*(2), 129-142.

Hanson, H., & Larson, M. (2008). Implications of extreme waves and water levels in the southern Baltic Sea. *Journal of Hydraulic Research*, *46*(sup2), 292-302. https://doi.org/10.1080/00221686.2008.9521962

Roberts, K. J., Pringle, W. J., & Westerink, J. J. (2019). OceanMesh2D 1.0: MATLAB-based software for two-dimensional unstructured mesh generation in coastal ocean modeling. *Geosci. Model Dev.*, *12*(5), 1847-1868. https://doi.org/10.5194/gmd-12-1847-2019

Rosenhagen, G., & Bork, I. (2009). Rekonstruktion der Sturmflutwetterlage vom 13. November 1872. *Die Küste*, *75*, 51-70.

Rosentau, A., Bennike, O., Uścinowicz, S., & Miotk ‐ Szpiganowicz, G. (2017). The Baltic Sea Basin. In (pp. 103-133). https://doi.org/10.1002/9781118927823.ch5

SGU. (2021). *Fysiska och dynamiska förhållanden längs Skånes kust - underlag för klimatanpassningsåtgärder (Appendix 1)*. T. S. G. S. (SGU).

Stanczak, G. (2008). *Breaching of sea dikes initiated from seaside by breaking wave impacts* University of Braunschweig]. Braunschwig.

Sukchaiwan, A. (2023a). *Analysis of waves during the 1872 storm on the south coast of Sweden*.

Sukchaiwan, A. (2023b). *Storm impact on dunes in the Falsterbo Peninsula* TU Delft]. not yet published.

Sweco. (2018a). *Bilaga B, Teknisk beskrivning - Bilaga till tillståndsansökan om översvämmningsskydd på Falsterbonäset* (13001214).

Sweco. (2018b). *Bilaga C11 - Meteorologiska Förutsättningar, Bilaga till tillståndsansökan om anläggande av översvämningsskydd på Falsterbohalvön*.

Sweco. (2018c). *Bilaga C, Miljökonsekvensbeskrivning - Bilaga till tillståndsansökan om översvämningsskydd på Falsterbohalvön* (13001214).

Zhong, H. (1985). Theoretische und experimentelle Untersuchungen ober den Druckschlag bei Wellenangriff auf einen 1:4 geneigten Seedeich. *Mitteilungen des Leichtweiß- Institut für Wasserbau, TU Braunschweig*, 401-453.